

## Revealing the Transition Dynamics from $Q$ Switching to Mode Locking in a Soliton Laser

Xueming Liu,<sup>1,4,5,6,\*</sup> Daniel Popa,<sup>2</sup> and Nail Akhmediev<sup>3</sup>

<sup>1</sup>*State Key Laboratory of Modern Optical Instrumentation, College of Optical Science and Engineering, Zhejiang University, Hangzhou 310027, China*


<sup>2</sup>*Department of Engineering, University of Cambridge, Cambridge CB3 0FA, United Kingdom*

<sup>3</sup>*Optical Sciences Group, Research School of Physics and Engineering, The Australian National University, Canberra 2600, Australian Capital Territory, Australia*

<sup>4</sup>*Institute for Advanced Interdisciplinary Research, Nanjing University of Aeronautics and Astronautics, Nanjing 210016, China*

<sup>5</sup>*College of Astronautics, Nanjing University of Aeronautics and Astronautics, Nanjing 210016, China*

<sup>6</sup>*School of Physics and Electronic Science, Hunan University of Science and Technology, Xiangtan 411201, China*

 (Received 5 February 2019; revised manuscript received 18 May 2019; published 27 August 2019)

$Q$  switching (QS) and mode locking (ML) are the two main techniques enabling generation of ultrashort pulses. Here, we report the first observation of pulse evolution and dynamics in the QS-ML transition stage, where the ML soliton formation evolves from the QS pulses instead of relaxation oscillations (or quasi-continuous-wave oscillations) reported in previous studies. We discover a new way of soliton buildup in an ultrafast laser, passing through four stages: initial spontaneous noise, QS, beating dynamics, and ML. We reveal that multiple subnanosecond pulses coexist within the laser cavity during the QS, with one dominant pulse transforming into a soliton when reaching the ML stage. We propose a theoretical model to simulate the spectrotemporal beating dynamics (a critical process of QS-ML transition) and the Kelly sidebands of the as-formed solitons. Numerical results show that beating dynamics is induced by the interference between a dominant pulse and multiple subordinate pulses with varying temporal delays, in agreement with experimental observations. Our results allow a better understanding of soliton formation in ultrafast lasers, which have widespread applications in science and technology.

DOI: [10.1103/PhysRevLett.123.093901](https://doi.org/10.1103/PhysRevLett.123.093901)

Ultrafast fiber lasers are increasingly used in a variety of applications, ranging from optical communications to sensors, medicine, and industry [1–9]. Their success is partly due to their ability to generate pulses with a wide range of parameters.  $Q$  switching (QS) and mode locking (ML) are the two main techniques used for pulse generation [10–14]. QS is a technique of modulation of the quality factor ( $Q$ ) of a laser cavity, where a pulse is formed when  $Q$  is high, thus allowing the stored energy to be released (lasing). This mechanism enables the formation of pulses with durations ranging from micro- to nanoseconds and repetition rates, typically around kilohertz, related to the lifetime of the gain medium [11]. On the other hand, ML enables the formation of a pulse by inducing a fixed phase relation (synchronization) among the oscillating modes of a laser cavity. Such mode interference leads to the formation of pulses with durations ranging from tens of picoseconds to sub-10 fs and repetition rates, typically around megahertz, given by the inverse of the cavity round-trip time ( $T_R$ ) [12]. Because of their shorter durations and higher peak intensities, in comparison to the QS pulses, ML pulses dictate stricter requirements to parameters of laser cavity. A common technique is a passive ML with an intracavity pulse (soliton) being shaped through a balance of cavity dispersion and pulse-triggered nonlinear effects [4,12].

Soliton lasers are being extensively investigated due to their highly stable operation and excellent pulse quality, placing them at the heart of ultrafast laser technology [1,15,16]. However, despite an increasing research effort dedicated to implementing QS and ML techniques in a variety of laser configurations [9,17–19], most pulse evolution and dynamics studies conducted in these systems are theoretical rather than experimental. Consequently, little is known about their real-time ultrafast transition dynamics [20–24].

The time-stretch dispersive Fourier transform (TSDFT) method is an emerging technique for studies of real-time transient processes in nonlinear optical systems. Here the spectrum of a broadband optical pulse is mapped, through dispersion, into a temporal waveform that can be subsequently digitized and processed in real time [25–31]. The TSDFT technique has been successfully employed to study the physical mechanisms of many important nonlinear phenomena in ultrafast optics. These include the transient dynamics of soliton molecules [28,32,33], internal motion of dissipative solitons [34,35], optical rogue waves [36], soliton explosions [37], and modulation instability in fiber lasers [38]. More recent experimental observations based on TSDFT techniques have shown that ML solitons appear from dominant picosecond fluctuations in a narrowband

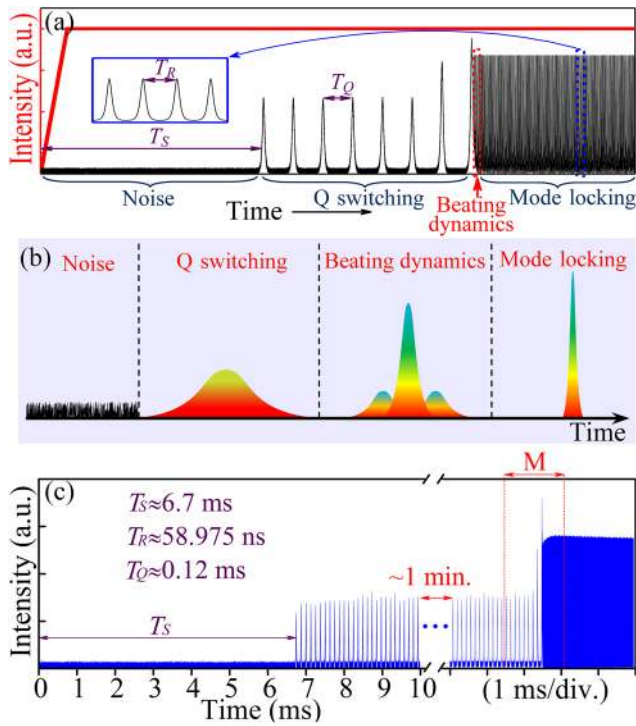


FIG. 1. Buildup process of solitons via QS. (a) Schematic diagram showing the transition from initial spontaneous noise, follow-up beating dynamics, and ML.  $T_S$ , start-up time;  $T_R$ , round-trip time of laser cavity;  $T_Q$ , time delay between two adjacent QS pulses (i.e., lasing spikes). (Inset) Time enlargement of ML stage. The pumping strength (red curve) increases rapidly ( $\sim 0.1$  ms) and remains constant afterwards. (b) Conceptual representation of the four soliton buildup stages. The QS pulse is 3–4 orders of magnitude longer than the ML soliton. Multiple pulses coexist during the beating dynamics stage, with one dominant pulse evolving into a soliton in the stable ML stage. (c) Experimental results of the entire buildup process of laser solitons. The time interval marked with red  $M$  is shown in detail in Fig. 3. The QS stage is characterized by many (e.g.,  $\sim 5 \times 10^5$  here) lasing spikes compared to a few (e.g., six in Ref. [32]) in the relaxation oscillation stage. Arbitrary units is denoted by a.u.

collection of many similar fluctuations [26,33], suggesting that they are formed from relaxation oscillations [32] and spectral beating dynamics [26]. However, beating dynamics is observed in the spectral domain only [26,32], and a theoretical model describing the physical mechanisms governing such dynamics is still missing.

By subtly designing the laser cavity and its components, here we report the first direct observation of soliton formation dynamics and its evolution in the transition phase from QS to ML. Using a TSDFT technique, we observe a new soliton buildup process, where solitons are generated via QS rather than from relaxation oscillations (or quasi-continuous-wave oscillations) as previously reported [26,32]. A schematic diagram of the transition, its conceptual representation, and experimental evidence are depicted in Figs. 1(a)–1(c), respectively. Four transition

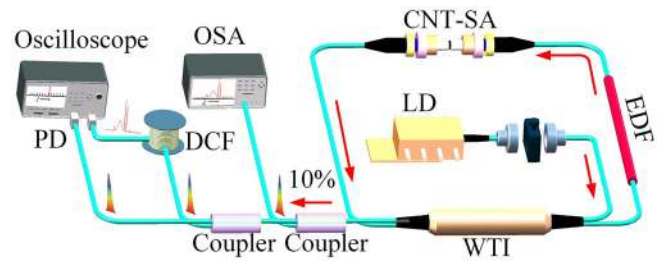


FIG. 2. Experimental setup containing a fiber laser oscillator for generating ML solitons via QS and a TSDFT setting for real-time measurements.

stages are shown, starting from initial spontaneous noise, successively experiencing QS, beating dynamics, and ML. Moreover, we propose a theoretical model to simulate the soliton formation through beating dynamics in both spectral and temporal domains.

The experimental setup, containing a fiber laser oscillator and a TSDFT setting, is shown in Fig. 2. We use a ring-configured oscillator composed of a polarization-insensitive carbon nanotube saturable absorber (CNTSA), a 3.5-m-long birefringent erbium-doped fiber (EDF),  $\sim 8.5$  m of single-mode fiber (SMF), and a hybrid combiner (WTI) (composed of a wavelength division multiplexer, a tap coupler, and an isolator). The EDF, with 6 dB/m absorption at 980 nm, is used as a gain medium. The WTI is used to ensure the unidirectional operation as the laser output and as the input for the pump [provided by a laser diode (LD)]. The oscillator has a fundamental frequency (repetition rate) of  $\sim 16.956$  MHz, corresponding to a  $T_R \sim 58.975$  ns. The real-time and time-averaged spectral data are recorded with a high-speed real-time oscilloscope via a photodetector (PD) and an optical spectrum analyzer (OSA), respectively. The TSDFT technique is implemented by temporally stretching the pulses through a 5.1-km-long dispersion-compensating fiber (DCF) with a dispersion of  $\sim -160$  ps/(nm km).

The QS-ML transition phase is quite sensitive to the characteristics of CNTSA and the laser cavity length  $L_{\text{cavity}}$ . Here,  $L_{\text{cavity}} \approx 12$  m and the CNTSA film has a modulation depth of  $\sim 10\%$  and a nonsaturable loss of  $\sim 60\%$ . When  $L_{\text{cavity}} > \sim 25$  m, the QS-ML transition vanishes, while the multisoliton operation appears. When the modulation depth and the nonsaturable loss of CNTSA are  $\sim 12\%$  and  $\sim 50\%$ , respectively, the relaxation oscillation occurs instead of QS. To achieve the QS-ML transition phase, therefore, the laser cavity together with CNTSA has to be designed accurately.

Figure 1(c) shows the experimental results recorded over the entire buildup process of solitons from spontaneous noise to ML via QS. The pump power is connected to the laser cavity at time  $T = 0$ . The population inversion increases in the gain medium when  $0 < T < \sim 6.7$  ms ( $T_S$  in Fig. 1). The photon number defined by the quantum field fluctuations initially remains low [10]. Stimulated emission becomes dominant afterwards, resulting in

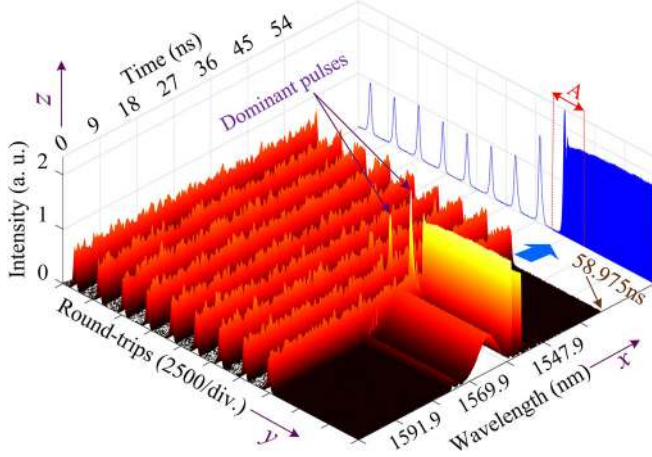


FIG. 3. Experimental real-time data of the soliton buildup process in the QS-ML transition phase, corresponding to the time interval  $M$  in Fig. 1(c). The shot-by-shot experimental data before and after the transition phase illustrate the temporal and spectral information, respectively. The intensity profile of pulses ( $z$  axis) evolves along with the round-trips ( $y$  axis) and the intracavity time ( $x$  axis). The blue projection on the  $y$  and  $z$  plane shows the intensity profile along with the round-trips, with a close-up (marked as range A) shown in Fig. 4 for details.

generation of QS pulses. Note that the spacing between two adjacent pulses,  $T_Q \approx 0.12$  ms, is uniform in the QS stage. In contrast, the spacing is nonuniform in Refs. [10,32], which is clear evidence of relaxation oscillations. A QS stage usually lasts for tens of seconds [ $\sim 1$  min. in Fig. 1(c)] with the pulsing period being random. Conversely, the relaxation oscillations with lasing spikes last less than 1 ms [32]. The comparison and differences between the QS and relaxation oscillations are presented in Fig. S1 in the Supplemental Material [39]. We have found that both  $T_S$  and  $T_Q$  are dependent on the pump power, shown in Fig. S2 in the Supplemental Material [39].

We analyze the shot-by-shot experimental data by segmenting the TSDFT recorded time series with a  $T_R = 58.975$  ns periodicity. The time interval  $M$  in Fig. 1(c) is redrawn as a spectrotemporal picture, shown in Fig. 3. The  $x$  axis in this plot depicts the time within a single round-trip (i.e., from 0 to 58.975 ns), while the  $y$  axis shows the dynamics across consecutive round-trips. Multiple subnanosecond pulses with different peak powers coexist in the cavity during this stage, as shown in Fig. 4(d) and Fig. S3 (see Supplemental Material [39]).

The A region in Fig. 3 (i.e., QS-ML transition phase) is magnified in Fig. 4(a) and further magnified in Fig. 4(b) (B region), in order to see clearly the beating pattern. Kelly sidebands do not appear during the first 40 round-trips [see Fig. 4(b)] of the QS-ML transition phase. They pop up together with the beating pattern. Multiple sidebands grow gradually and simultaneously. These features are characteristic of solitons [6]. They are not formed at the early stage of the transition phase, although the QS pulses exist at this

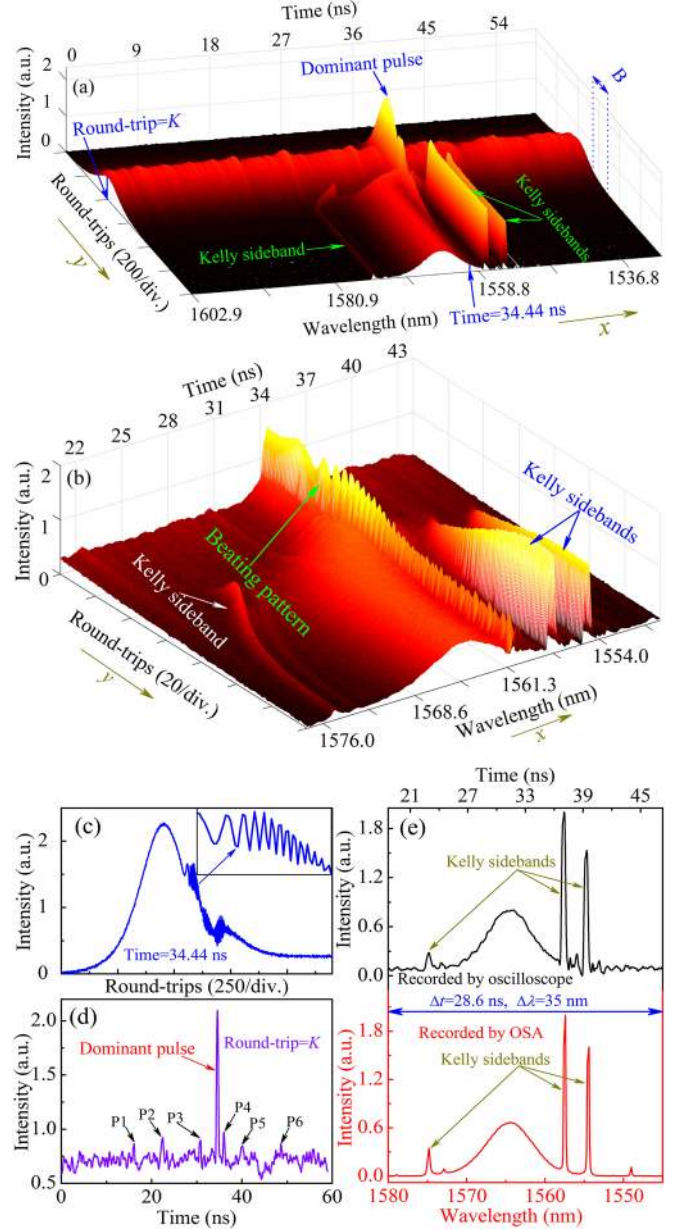


FIG. 4. Details of the transition phase from QS to ML. (a) Magnification of the region A in Fig. 3. (b) Magnification of the region B in (a), showing a detailed beating pattern and the growth of Kelly sidebands. (c) The cross section of  $x$  axis in (a) at 34.44 ns intracavity time. (Inset) Beating dynamics magnification. (d) The cross section of  $y$  axis in (a) at the round-trip  $K$ . It shows the competing of the dominant pulse with multiple subordinate pulses denoted as P1–P6. (e) Optical spectrum of solitons recorded by OSA (red curve) and an exemplary single-shot spectrum (black curve) recorded by our high-speed real-time oscilloscope (TSDFT setting), corresponding to the last frame in (a).

stage as Fig. 4(b) shows. This process is depicted in Figs. 4(c) and 4(d) for cross sections marked at 34.44 ns along the  $x$  axis and  $K$  along the  $y$  axis in Fig. 4(a). A modulation pattern, which is a result of beating dynamics,

can be seen in the inset of Fig. 4(c). Multiple subnanosecond pulses appear at the QS stage, as shown in Fig. 4(d) and in Fig. S3 of the Supplemental Material [39], with one dominant pulse eventually evolving into a stationary soliton in the ML stage [Fig. 4(a)]. Using the TSDFT technique, femtosecond pulses can be broadened to nanosecond pulses, while pulses over tens of picoseconds are hardly broadened [32]. As a result, subnanosecond pulses do exist in the first 40 round-trips in Fig. 4(b), while femtosecond ML solitons appear only in the subsequent round-trips. A full animation of this evolution in the real-time experimental observation of the QS-ML transition phase is shown in the video of the Supplemental Material [44].

Figure 4(e) shows the soliton optical spectrum (red curve) and an exemplary single-shot spectrum (black curve), recorded by the OSA and the high-speed real-time oscilloscope, respectively. The two curves (including Kelly sidebands) are consistent, giving a  $\Delta\lambda = 35$  nm bandwidth for the optical spectrum mapped (stretched) over a  $\Delta t = 28.6$  ns time spacing. The mapping relation between spectral and temporal domains can be expressed as  $\Delta t = |D|L\Delta\lambda$  [29,32], where  $D$  is the dispersion parameter and  $L$  is the length of the DCF, with  $D \sim -160$  ps/(nm km) and  $L \sim 5100$  m (see Fig. 1) in our experiments. If the TSDFT technique is not used, the beating phenomenon and Kelly sidebands cannot be discovered, just as in the previous report [32].

To better understand the soliton dynamics and its formation, we perform numerical simulations based on a round-trip circulating-pulse method [40]. To discover the beating behavior, we consider the influence of the nonlinear refractive index defined by the second term of Eq. (1), which can cause the temporal delays of pulses. We use a modified nonlinear Schrödinger equation (MNSE) for simulating a propagating pulse through an optical fiber, given by (see the Supplemental Material [39] for the detailed derivation)

$$\begin{aligned} \frac{\partial A}{\partial z} + \frac{\gamma\lambda_0|A|^2}{2\pi c} \frac{\partial A}{\partial T} + \frac{i\beta_2}{2} \frac{\partial^2 A}{\partial T^2} - \frac{\beta_3}{6} \frac{\partial^3 A}{\partial T^3} \\ = \frac{g}{2} A + i\gamma|A|^2 A + \frac{g}{2\Omega_g^2} \frac{\partial^2 A}{\partial T^2}. \end{aligned} \quad (1)$$

Here  $A$ ,  $\lambda_0$ ,  $c$ , and  $\gamma$  represent the pulse electric field envelope, its central wavelength, the speed of light in vacuum, and the fiber cubic refractive nonlinearity, respectively.  $\beta_2$  and  $\beta_3$  are the fiber second- and third-order dispersion coefficients, respectively. To simplify the MNSE, a frame of reference moving with the pulse at the group velocity  $v_g$  is used by making the transformation  $T = t - z/v_g$  [41], where  $t$  and  $z$  are the time and the propagation distance variables, respectively. We use  $g = g_0 \exp(-E_p/E_s)$  to describe the EDF gain (note that  $g = 0$  for SMF), where  $g_0$  is the small-signal gain coefficient,  $E_p$

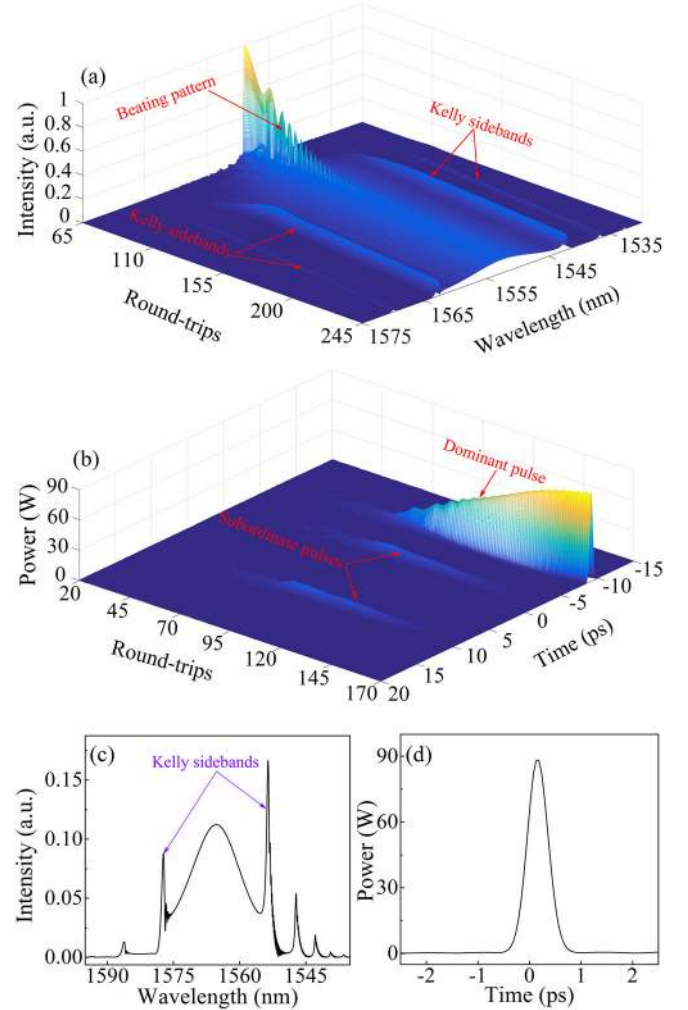


FIG. 5. Numerical simulations revealing the soliton formation through beating dynamics. (a) Spectral and (b) temporal evolutions in the soliton buildup process. The phenomena of spectral beating and Kelly sidebands are clearly seen. Multiple (two in this case) subordinate pulses play key roles in the beating pattern. The disappearance of subordinate pulses will terminate the beating dynamics described as auxiliary-pulse ML in Ref. [26]. (c) Spectral and (d) temporal profiles of stationary solitons.

is the pulse energy, and  $E_s$  is the gain saturation energy [40,41]. In our simulations, we start with an initial small signal as noise background, as shown in Fig. S5 in the Supplemental Material [39]. This initial signal is nearly 8 orders of magnitude weaker than the stable soliton. To match the experimental conditions, we use the following parameters:  $\Omega_g = 40$  nm,  $\beta_3 = 0.3$  ps<sup>3</sup>/km,  $\lambda_0 = 1565$  nm,  $E_s = 90$  pJ;  $\beta_2 = 13.5$  ps<sup>2</sup>/km and  $\gamma = 1.8$  W<sup>-1</sup> km<sup>-1</sup> for EDF;  $\beta_2 = -21.7$  ps<sup>2</sup>/km and  $\gamma = 1$  W<sup>-1</sup> km<sup>-1</sup> for SMF.

The spectral and temporal evolutions of soliton formation are shown in Figs. 5(a) and 5(b). The stable solutions at 700 round-trips are shown in Figs. 5(c) and 5(d) in the spectral and temporal domains, respectively. Our numerical model clearly reveals the spectral beating behavior and

Kelly sidebands [see Fig. 5(a)]. Like in the experimental observations, spectra are narrow and no Kelly sideband appears at the early stage of beating dynamics (below 100 round-trips). They broaden rapidly afterwards with Kelly sidebands increasing simultaneously. The sidebands are asymmetrical due to the third-order dispersion term  $\beta_3$  [see Eq. (1)]. The numerical results are in good agreement with the experimental observations shown in Fig. 4(b). To simplify MNSE, the EDF birefringence is omitted in Eq. (1).

Our numerical simulations confirm that the beating pattern phenomenon originates from the interference of multiple pulses with varying temporal delays induced by the nonlinear refractive index and the dispersion. The second term in Eq. (1) plays an important role in the occurrence of the beating pattern, which can induce varying pulse delay. The spectral amplitude can be obtained, via Fourier transform, from the temporal amplitude of all the pulses accompanied by their respective temporal delays. As a result, the pattern in the spectral regime demonstrates the beating behavior. Numerical results show that beating dynamics occurs in the region from  $\sim 40$  to 170 round-trips [see Figs. 5(a) and 5(b)], due to the temporal delays of these pulses. A dominant pulse is seen together with multiple (two in this case) subordinate pulses during the beating dynamics process, with the disappearance of the subordinate pulses terminating such process. The dominant pulse has a relatively low power and large duration during the early stage ( $\sim 40$ –80 round-trips) of the buildup process [see Fig. 5(b)], corresponding to a sharp Fourier transformed spectral peak with narrow bandwidth [see Fig. 5(a)]. Such pulse then increases its power and shortens its duration along with the round-trips and simultaneously reduces its spectral peak and broadens its spectral bandwidth. After  $\sim 170$  round-trips, the two subordinate pulses die away [see Fig. 5(b)] and the spectral beating pattern vanishes [see Fig. 5(a)].

The numerical calculations show that both the nonlinear refractive index and the dispersion can cause the time delay of respective pulses. When the nonlinear refractive index is excluded from Eq. (1), the beating pattern [see Fig. 5(a)] will be weakened and blurred. In this case, the numerical results deviate from the experimental observations.

In conclusion, by using a TSDFT technique, we reveal the real-time soliton buildup process in the ultrafast laser cavity that transforms the initial spontaneous noise into stable ML (via QS). We experimentally observe, for the first time to our best knowledge, the single-shot dynamics and evolution of solitons from QS to ML transition phase. A new way of soliton buildup in lasers is discovered, where solitons are generated by ML via QS, rather than from relaxation oscillations or quasi-continuous-wave oscillations as previously reported [26,32]. It is revealed that multiple subnanosecond pulses coexist in the laser cavity during the QS stage, with one dominant pulse transitioning

into a soliton of the stable ML stage. We propose a theoretical model to reveal the soliton formation through the QS-ML transition phase (characterized as beating dynamics), thus validating the experimental results. The numerical results show that a dominant pulse together with multiple subordinate pulses induces the spectral beating dynamics, which plays the key role in the buildup process of solitons. Both theoretical and experimental results confirm that the beating behavior is an inevitable phenomenon in the formation of mode-locked lasers [26,32,39]. Our findings open new perspectives for ultrafast transient dynamics and pathways of pulse evolution and will bring new insights into the design and application of lasers.

We thank Y. Zhang, X. Yao, C. Jin, and J. Zhen for fruitful discussions. This Letter was partially supported by the National Natural Science Foundation of China under Grants No. 61525505 and No. 11774310.

---

\*liuxueming72@yahoo.com

- [1] U. Keller, *Nature (London)* **424**, 831 (2003).
- [2] L. G. Wright, D. N. Christodoulides, and F. W. Wise, *Science* **358**, 94 (2017).
- [3] M. Pang, W. He, X. Jiang, and P. S. J. Russell, *Nat. Photonics* **10**, 454 (2016).
- [4] P. Grelu and N. Akhmediev, *Nat. Photonics* **6**, 84 (2012).
- [5] J. M. Dudley, F. Dias, M. Erkintalo, and G. Genty, *Nat. Photonics* **8**, 755 (2014).
- [6] H. A. Haus and W. S. Wong, *Rev. Mod. Phys.* **68**, 423 (1996).
- [7] D. V. Churkin, S. Sugavanam, N. Tarasov, S. Khorev, S. V. Smirnov, S. M. Kobtsev, and S. K. Turitsyn, *Nat. Commun.* **6**, 7004 (2015).
- [8] A. Klein, G. Masri, H. Duadi, K. Sulimany, O. Lib, H. Steinberg, S. A. Kolpakov, and M. Fridman, *Optica* **5**, 774 (2018).
- [9] B. Oktem, C. Ülgüdür, and F. Ö. Ilday, *Nat. Photonics* **4**, 307 (2010).
- [10] O. Svelto, *Principles of Lasers* (Plenum, New York, 1998).
- [11] D. Popa, Z. Sun, T. Hasan, F. Torrisi, F. Wang, and A. C. Ferrari, *Appl. Phys. Lett.* **98**, 073106 (2011).
- [12] G. P. Agrawal, *Applications of Nonlinear Fiber Optics* (Academic Press, San Diego, 2008).
- [13] S. A. Kolpakov, H. Khashi, and S. V. Sergeyev, *Optica* **3**, 870 (2016).
- [14] C. M. Eigenwillig, W. Wieser, S. Todor, B. R. Biedermann, T. Klein, C. Jirauschek, and R. Huber, *Nat. Commun.* **4**, 1848 (2013).
- [15] M. E. Fermann and I. Hartl, *Nat. Photonics* **7**, 868 (2013).
- [16] J. Gabzdyl, *Nat. Photonics* **2**, 21 (2008).
- [17] K. Sulimany, O. Lib, G. Masri, A. Klein, M. Fridman, P. Grelu, O. Gat, and H. Steinberg, *Phys. Rev. Lett.* **121**, 133902 (2018).
- [18] D. Chaparro and S. Balle, *Phys. Rev. Lett.* **120**, 064101 (2018).
- [19] A. H. Quarterman, K. G. Wilcox, V. Apostolopoulos, Z. Mihoubi, S. P. Elsmere, I. Farrer, D. A. Ritchie, and A. Tropper, *Nat. Photonics* **3**, 729 (2009).

- [20] M. Kues, C. Reimer, B. Wetzel, P. Roztock, B. E. Little, S. T. Chu, T. Hansson, E. A. Viktorov, D. J. Moss, and R. Morandotti, *Nat. Photonics* **11**, 159 (2017).
- [21] W. Liang, V. S. Ilchenko, A. A. Savchenkov, A. B. Matsko, D. Seidel, and L. Maleki, *Phys. Rev. Lett.* **105**, 143903 (2010).
- [22] M. Leonetti, C. Conti, and C. Lopez, *Nat. Photonics* **5**, 615 (2011).
- [23] X. Liu, *Phys. Rev. A* **81**, 023811 (2010).
- [24] A. Chong, L. Wright, and F. Wise, *Rep. Prog. Phys.* **78**, 113901 (2015).
- [25] K. Goda, K. K. Tsia, and B. Jalali, *Nature (London)* **458**, 1145 (2009).
- [26] G. Herink, B. Jalali, C. Ropers, and D. R. Solli, *Nat. Photonics* **10**, 321 (2016).
- [27] A. Tikan, S. Bielawski, C. Szwaj, S. Randoux, and P. Suret, *Nat. Photonics* **12**, 228 (2018).
- [28] G. Herink, F. Kurtz, B. Jalali, D. R. Solli, and C. Ropers, *Science* **356**, 50 (2017).
- [29] Y. C. Tong, L. Y. Chan, and H. K. Tsang, *Electron. Lett.* **33**, 983 (1997).
- [30] M. A. Muriel, J. Azaña, and A. Carballar, *Opt. Lett.* **24**, 1 (1999).
- [31] C. Lei and K. Goda, *Nat. Photonics* **12**, 190 (2018).
- [32] X. Liu, X. Yao, and Y. Cui, *Phys. Rev. Lett.* **121**, 023905 (2018).
- [33] J. Peng and H. Zeng, *Laser Photonics Rev.* **12**, 1800009 (2018).
- [34] K. Krupa, K. Nithyanandan, U. Andral, P. Tchofo-Dinda, and P. Grelu, *Phys. Rev. Lett.* **118**, 243901 (2017).
- [35] P. Ryczkowski, M. Närhi, C. Billet, J. M. Merolla, G. Genty, and J. M. Dudley, *Nat. Photonics* **12**, 221 (2018).
- [36] D. R. Solli, C. Ropers, P. Koonath, and B. Jalali, *Nature (London)* **450**, 1054 (2007).
- [37] A. F. J. Runge, N. G. R. Broderick, and M. Erkintalo, *Optica* **2**, 36 (2015).
- [38] D. R. Solli, G. Herink, B. Jalali, and C. Ropers, *Nat. Photonics* **6**, 463 (2012).
- [39] See Supplemental Material at <http://link.aps.org/supplemental/10.1103/PhysRevLett.123.093901> for more detailed discussions, which includes Refs. [10,11,26,32,40–43]. Section 1 compares the  $Q$  switching and relaxation oscillations. Section 2 describes the start-up time and repetition rate of  $Q$  switching versus pump power. Section 3 magnifies three lasing spikes preceding the formation of stable ML solitons. Section 4 compares optical spectra of QS and ML pulses. Section 5 describes the proposed theoretical model in detail. Section 6 illustrates the initial signal with the noise background. Section 7 demonstrates the evolution from many pulses to a soliton via beating behavior.
- [40] X. Liu, Y. Cui, D. Han, X. Yao, and Z. Sun, *Sci. Rep.* **5**, 9101 (2015).
- [41] G. P. Agrawal, *IEEE Photonics Technol. Lett.* **2**, 875 (1990).
- [42] B. Dong, C. Liaw, J. Hao, and J. Hu, *Appl. Opt.* **49**, 5989 (2010).
- [43] G. P. Agrawal, *Nonlinear Fiber Optics* (Academic Press, San Diego, 2007).
- [44] See Supplemental Material at <http://link.aps.org/supplemental/10.1103/PhysRevLett.123.093901> for a video showing the experimental real-time measurements from DCF (i.e., with time-stretch technique) for the transition dynamics.